Nanotechnol. Environ. Eng. (2016) 1:10
DOI 10.1007/s41204-016-0010-7

ORIGINAL PAPER

Mesoporous MgO nanoparticles as a potential sorbent for removal of fast orange and bromophenol blue dyes

M. A. Ahmed[1] · **Z. M. Abou-Gamra**[1]

Received: 11 July 2016 / Accepted: 22 September 2016 / Published online: 4 October 2016
© Springer International Publishing Switzerland 2016

Abstract The removal of fast orange 3R and bromophenol blue dyes was successfully performed on mesoporous MgO nanoparticles. MgO nanoparticles were prepared by sol–gel route using CTAB as template agent. The crystalline, texture and the morphology feature of the prepared nanoparticles were investigated using X-ray diffraction, adsorption–desorption isotherm, scanning electron microscope, transmission electron microscope and high resolution transmission electron microscope. The results showed that the formation of nanorods of average size about 24 nm in diameter and 38 nm in length. Adsorption of both dyes changed crystallography of catalyst from cubic MgO to hexagonal $Mg(OH)_2$. This research work investigated the factors affecting dye uptake such as contact time, catalyst dosage, initial dye concentration and temperature. Different types of adsorption isotherms and kinetic models were performed to get a clear picture on the mechanism and the kinetic of the adsorption process. Thermodynamic parameters such as free energy, entropy and enthalpy were estimated. The experimental results showed that the adsorption equilibrium data are fitted well to the Langmuir and Freundlich isotherms. The adsorption isotherms indicated that the adsorption capacities are 30 and 40 mg g^{-1} for fast orange and bromophenol blue, respectively. The adsorption processes follow pseudo-second-order rate equation. Enthalpy change ($\Delta H°$) for fast orange and bromophenol blue dye is +37.8 and +7.3 kJ mol^{-1}, respectively, indicating that the removal processes are endothermic. The negative values of free energy ($\Delta G°$) suggested that the adsorption processes are spontaneous.

Keywords MgO nanoparticles · Phase transformation · Fast orange · Bromophenol blue

Introduction

The discharge of dyes and colored organic particles comes from textiles, plastics, paper, leather, food and cosmetic industries which are considered one of the major sources of water pollution [1–3]. These organic dyes with deeply color are very stable and difficult to decompose by various techniques. The toxicity and the carcinogenic effect of these dyes are considered an obstacle for reusing the wastewater for various purposes [3, 4]. Therefore, the removal of these organic pollutants is considered one of the main environmental challenges during the recent years.

Many technologies were performed to remove these pollutants using low costs and non-toxic materials as adsorption, coagulation, flocculation, reverse osmosis, biological and photocatalytic methods [4]. Unfortunately, the photocatalysts are expensive and may lead to transfer the primary pollutants to secondary one that requires further treatment. Biotechnology methods use microbes and other low cost naturally occurring materials are costly, energy demanding and generating large quantities of sludge. Adsorption was revealed as the most promising and widely used method for the removal of both inorganic and organic pollutants from contaminated water [5–11]. Activated carbon of higher surface area and adsorption capacity was involved extensively in removal of various toxic organic pollutants [12]. However, high cost of activated

✉ Z. M. Abou-Gamra
zanibabougamra@yahoo.com

M. A. Ahmed
abdelhay71@hotmail.com

[1] Chemistry Department, Faculty of Science, Ain Shams University, Cairo, Egypt

carbon limits its application on a large industrial scale. Many researches are concerned with development of novel adsorbents with high adsorptive capacity and low cost. Great attention has been paid to nanotechnology [13, 14]. This is due to nanomaterials have large surface areas that can attract large number of dyes molecules to be adsorbed on its surface.

MgO as a versatile oxide material exhibits wide band gap, high thermodynamic stability, low dielectric constant and low refractive index is considered a promising oxide with wide industrial applications [14]. MgO nanoparticles [15, 16] are very promising as new adsorbent owing to its destructive sorbent, high surface reactivity and adsorption capacity compared with other metal oxides as ZnO, TiO_2 and Al_2O_3. MgO oxide is more specific for removal of anionic organic compounds through electrostatic attraction between anionic compound and positive charged catalyst surface (point of zero charge = 12.4) [17]. Li et al. [18] prepared mesoporous MgO by hydrothermal process using dioctylsulfosuccinate sodium surfactant for removing various organic dyes as Congo red (471–588 mg g^{-1}), Methyl orange (370 mg g^{-1}) and Sudan III (180 mg g^{-1}). They attributed the high reactivity of samples to their mesoporous structures which facilitate the mass diffusion in pores and allow the dye molecules to contact the adsorptive sites more easily. Moussavi and Mahmoudi [4] prepared porous MgO of particle size in the range of 38–44 nm, with an average specific surface area of 153.7 m^2/g for removal of reactive blue 19 and reactive red 198 dyes as model azo and anthraquinone dyes. Their results indicated that the prepared MgO powder can remove more than 98 % of both dyes under optimum operational conditions of a dosage of 0.2 g, pH = 8 and a contact time of 5 min for initial dye concentrations of 50–300 mg L^{-1}. Venkatesha et al. [19] prepared MgO nanoparticles by precipitation method and used for the sorption of Ponceau S from aqueous solution. They indicated that adsorption was more favorable at neutral pH and electrostatic forces of attraction were responsible for high adsorption capacity of MgO. Venkatesha et al. [20] investigated the removal of Levafix Fast Red CA (LFR) and Indanthrene Blue BC (IB) dyes on the surface of MgO nanoparticles of crystallite size in the range of 25–30 nm. The adsorption process fitted Langmuir adsorption isotherm with high correlation coefficients and the kinetic modeling suggested that pseudo-second-order model. Mahmoud et al. [21] prepared Fe_2O_3/MgO nanomaterials by impregnation, co-precipitation and hydrothermal methods for removal Remazol dye from aqueous solution. The results indicated that the hydrothermal method is the most effective one in creating highly adsorbed nanoparticles and the pseudo-first-order and intraparticle diffusion models are successfully described the adsorption kinetics. Wang et al. [22]. reported that hierarchical porous nanosheet-assembled MgO is effective for removal Congo red dye three times higher than that of MgO microrods. It should be emphasized that the efficiency of metal oxide in removal of toxic pollutants through adsorption process is mainly influenced by the surface area, particle and pore structure which can be adjusted by controlling the preparation steps.

Therefore, this research work focused on preparation of MgO nanoparticles by sol–gel route using CTAB template as controlling template to manipulate rod nanoparticles with mesoporous structure. This research work concerned with investigation of the reactivity of novel mesoporous MgO nanoparticles in removal of fast orange and bromophenol blue. The structural and crystalline features of the synthesized sample were performed by XRD techniques. However, the morphology and nanostructure were investigated by SEM, TEM and HRTEM. The removal of the dyes was studied over wide range of dye concentrations and different dosage of catalyst sample. Adsorption isotherms were studied using Freundlich, Langmuir, Temkin and Dubinin models to indicate the mechanism of adsorption and estimate the maximum adsorption capacity and correlation coefficients. The kinetics of adsorption process was investigated using different models as pseudo-first order, pseudo-second order, Elovich, Morris and Weber.

Experimental

Materials

All chemicals including $MgCl_2 \cdot 2H_2O$, Fast orange 3R, bromophenol blue, Malachite green dyes and ammonia solution, CTAB (cetyltrimetyl ammonium bromide) with the highest purity were purchased from Sigma–Aldrich. Table 1 represents the general characteristics of dyes under investigation.

Preparation of mesoporous MgO nanopowders

MgO nanoparticles were prepared by controlled sol–gel method as follows: About 10 mL of CTAB as cationic surfactant solution was added with constant stirring for 1 h to 500 mL of 1 M $MgCl_2$ solution. Afterwhile, ammonia solution [1 M] was added drop by drop until the clear solution changed to white sol of $Mg(OH)_2$. The sol was stirred for 2 h and left for 2 days for condensation of sol particles into gel. The gel particles were collected by filtration and washed with distilled water several times. After washing, the final product was dried at 100 °C for 24 h. The dried powders were calcined in high temperature

Table 1 Molecular structure of FO3R and BPB

Characteristic	Fast orange R	Bromophenol blue	Malachite green
	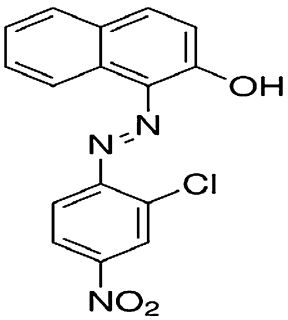	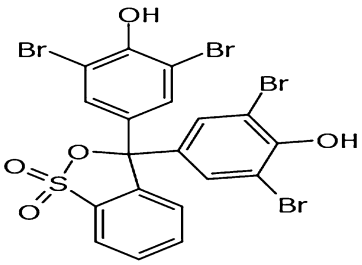	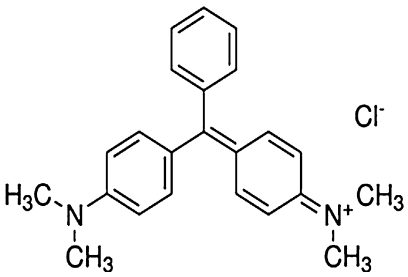
Chemical formula	$C_{16}H_{10}N_3O_3Cl$	$C_{19}H_{10}Br_4O_5S$	$C_{23}H_{25}ClN_2$
Molecular weight	327.72	669.96	364.911

furnace at 500 °C for 3 h to transform $Mg(OH)_2$ into MgO nanoparticles.

Measurements

X-ray diffraction patterns were carried out by XRD-6100 X-ray diffractometer, with CuK_α ($\lambda = 1.5406$ Å) radiation in the 2θ range from 5 to 90°. The scanning mode is continuous with scan speed 2° min^{-1}, the sampling pitch 0.02° and the preset time 0.6 s.

The surface morphology of MgO before and after adsorption was carried out by scanning electron microscope (JEOL, JEM-1200X II).

The nanostructure of MgO rods was investigated by transmission electron microscope (JEOL, JEM-1200X II) and high resolution transmission electron microscope.

Adsorption–desorption isotherms of purified N_2 at 77 K were determined using a conventional volumetric apparatus connected to a vacuum system that allowed prior outgassing to a residual pressure of 10^{-5} Torr.

Adsorption studies

Fast orange 3R, bromophenol blue and Malachite green as azo and triphenylmethane dyes, respectively, were taken as pollutants models to investigate the adsorption capacity of MgO nanoparticles.

The equilibrium isotherm of a specific adsorbent represents its adsorptive characteristics and is very important to the design of adsorption processes. Experiments for the estimation of the adsorption isotherms of fast orange 3R and bromophenol blue onto MgO nanoparticles were performed by adding fixed amounts of MgO powder to a series of Erlenmeyer flasks, each containing dye solutions of concentrations 17–83 and 1.8–38 mg L^{-1} for FO3R and BPB, respectively, at pH = 8.3. The vessels were then agitated using shaker for 90 min at room temperature to reach equilibrium. Then 5 mL of solutions were centrifuged for 5 min at 1800 rpm to remove adsorbent. Supernant concentrations were determined spectrophotometrically at $\lambda_{max} = 420$ nm and 580 nm for fast orange 3R and bromophenol blue, respectively. The amount of dye adsorbed onto MgO nanoparticles was calculated based on the following mass balance equation:

$$q_e = \frac{V(C_o - C_e)}{m}$$

where q_e is the adsorption capacity (mg dye adsorbed onto the mass unit of MgO, mg g^{-1}), V is the volume of the dye solution (L), C_o and C_e (mg L^{-1}) are initial and equilibrium dye concentrations and m (g) is the mass of dry MgO added. The equilibrium relationship between the quantity of adsorbate per unit of adsorbent (q_e) and its equilibrium solution concentration (C_e) at a constant temperature is known as the adsorption isotherm [23]. Several isotherm models have been developed for evaluating the equilibrium adsorption of compounds from solutions such as Langmuir, Freundlich, Dubinin–Radushkevich and Temkin. Moreover, the kinetics of dye adsorption is investigated using pseudo-first order, pseudo-second order, Elovich and Weber–Morris models.

Results and discussion

Addition of MgO to Malachite green solution increased the pH of solution to 10 due to high PZC (12.6) of MgO and the deep green color of Malachite changed to colorless within 30 min while MgO solid remained colorless. In

absence of MgO, Malachite green involved in decolorization by increasing the pH of solution to 10 by adding NaOH with rate constant equals to rate constant of Malachite in presence of MgO as presented in Fig. 1. This is attributed to hydroxyl ion coverts Malachite to Carbinol base with no conjugation structure (Scheme 1), i.e., decolorization of Malachite resulted from change in pH instead of adsorption on MgO. Consequently, Malachite green is excluded from this study.

XRD

XRD analysis is performed to investigate the crystalline features of the prepared MgO and to study the influence of dye adsorption on the crystalline parameters of MgO as presented in Fig. 2. The XRD peaks at various $2\theta = 37.1$, 44.0, 62.4, 74.8 and 78.6 are assigned to (111), (200), (220), (311) and (222) reflections according the JCDPS card No. (89-4248) [24]. The diffraction pattern matched with the face centered cubic structure of periclase MgO (JCPDS No. 87-0653). On examining Fig. 2, one can notice that the broadness of the diffraction peaks revealing the successful role of the preparation route in preventing the crystal growth during the progress of calcination. It is obvious to notice that the XRD patterns of MgO nanoparticles after adsorption of dyes belong to $Mg(OH)_2$ with (100), (101), (102), (110) planes revealing the full hydration of MgO nanoparticles during the process of dye adsorption. This facility of hydration of MgO particles is reported by various authors [25]. Using Scherrer equation, the estimated crystallite size of pure MgO and MgO after adsorption of FO3R and BPB was 22, 16 and 11 nm, respectively. This result reveals the successful preparation route in fabricating crystallites in nanodimensions.

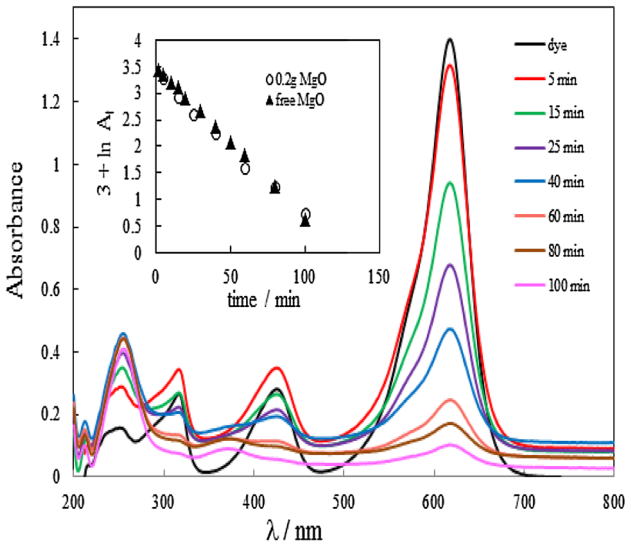

Fig. 1 UV-Vis spectrum of Malachite green with 0.2 g of MgO, inset, first-order plots for Malachite green in presence and absence MgO. [MG] = 2.5×10^{-5} mol dm^{-3}, pH = 10.5, Temp. = 25 °C

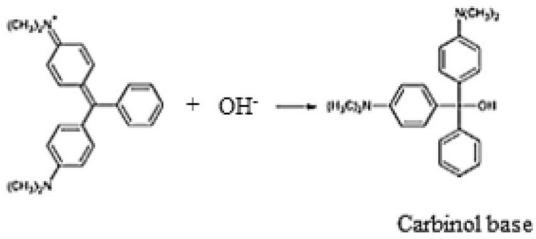

Scheme1 Discoloration of Malachite Green in basic medium

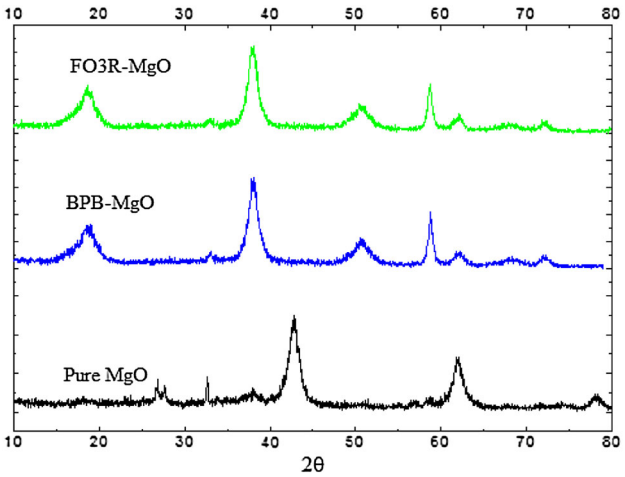

Fig. 2 XDR pattern of MgO nanoparticles before and after adsorption of FO3R and BPB

SEM

The micrograph of MgO sample as presented in Fig. 3 reveals the existence of large number of tiny wires with nearly homogeneous structure dispersed through the whole sample matrix. It is interesting to notice that the adsorption of both dyes affects the particles distribution and increases the tendency of the particles for agglomeration. This tendency is more pronounced in adsorption of FO3R rather than BPB in which the particles is completely compact through the matrix of sample. This may be due to the chemical bonding that linked MgO with FO3R and BPB dyes.

HRTEM

The transmission electron microscope (TEM), high resolution transmission electron microscope (HRTEM) and the selected area electron diffraction (SAED) were performed to investigate the nanostructure of MgO nanoparticles as presented in Fig. 4a–c. Figure 4a indicates the existence of

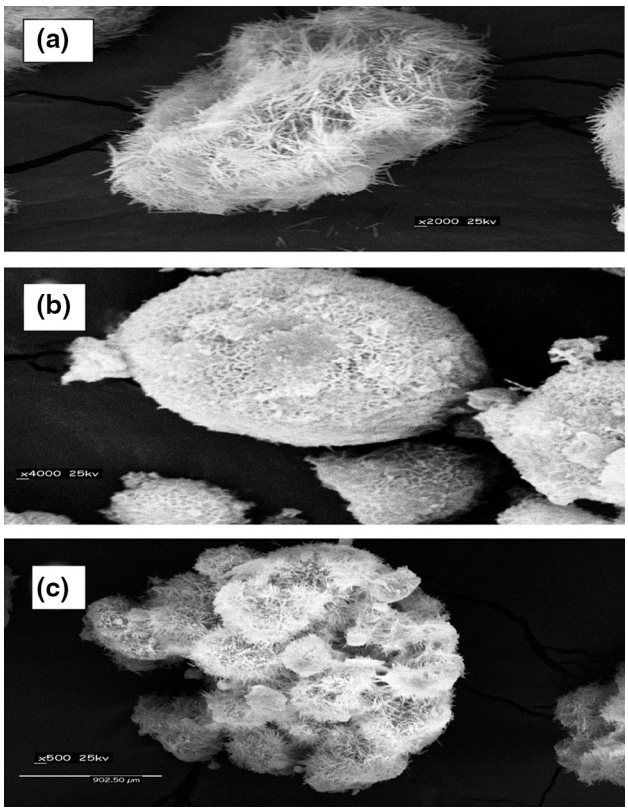

Fig. 3 SEM micrographs of MgO nanoparticles **a** before adsorption, **b** after adsorption of FO3R, **c** after adsorption of BPB

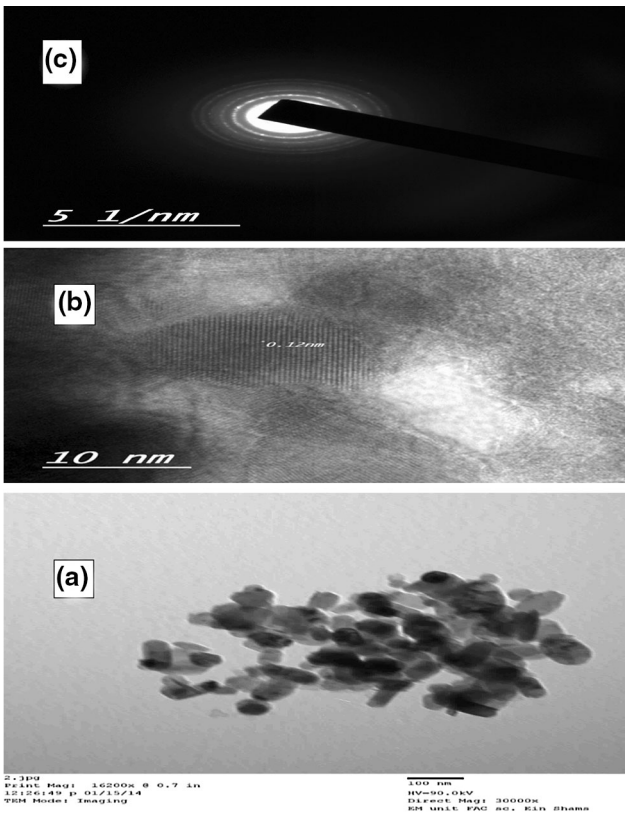

Fig. 4 TEM, HRTEM and SAED micrographs of MgO nanoparticles **a** TEM, **b** HRTEM, **c** SAED

nanorods with various sizes. Various authors were pointed the formation of MgO nanorods through different routes of preparation [21, 22, 26, 27]. It is clearly observed the homogeneous distribution of the prepared nanorods through the whole matrix. The HRTEM image reflected the existence of MgO nanoparticles in crystalline structure, and the spacing between two lattice planes is 0.12 nm can be due to the adjacent (200) planes of cubic MgO as presented in Fig. 4b. Figure 4c displays the SAED pattern of MgO, and the observed diffraction rings in SAED pattern clearly indicate high crystallinity of the sample. These diffraction rings were indexed to (111), (200), (220), (311) and (222) planes and were attributed to cubic phase of MgO.

Textural characterization of MgO nanoparticles

Figure 5 illustrates the adsorption–desorption isotherms of N_2 adsorption at 77 K on MgO nanoparticles. The adsorption isotherm is classified as type IV according to IUPAC is generally attributed to pores of narrow entrances and wider bodies-ink bottle shape. The specific surface area (A_{BET}) of the prepared sample is about 108.34 m^2/g which was estimated by using the BET equation in its normal range of applicability and adopting a value of 16.2 Å for

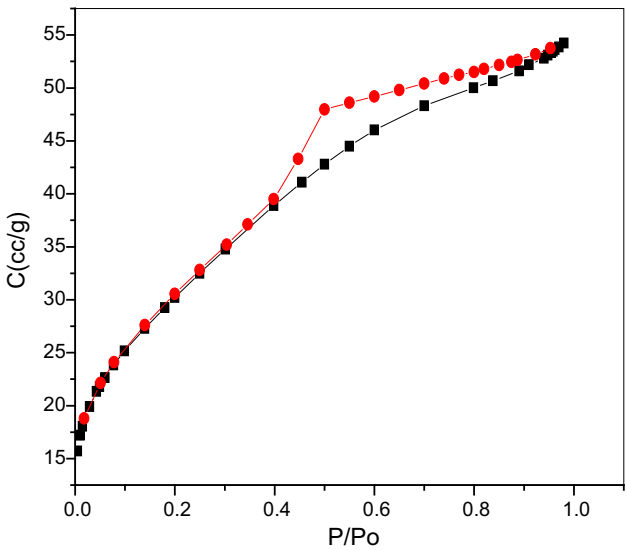

Fig. 5 Adsorption–desorption isotherm of N_2 gas on MgO

the cross-sectional area of N_2. However, the total pore volume (Vp) was taken at a saturation pressure and expressed as liquid volume = 0.0839 cc/g. The average pore radius = 30.09 Å which reveals that a sample is in lower stage of mesoporosity.

Dye adsorption analysis

Effect contact time

Equilibrium time is one of the important parameters to design a low cost adsorbent for removal of organic wastes. The adsorption of FO3R and BPB dyes onto MgO at constant pH = 8.3 was studied as a function of contact time to determine the necessary adsorption equilibrium time as presented in Fig. 6. Figure 6 showed that about 75–80 % of both dyes was adsorbed in 75 min and attaining the equilibrium at 90 min.

Effect of MgO dose

The amount of solid catalyst is important parameter for detection of adsorption capacity of solid in removing organic wastes. A rapid uptake of pollutants and establishment of equilibrium in a short period mean the efficiency of the solid in removal of various organic pollutants. The effect of MgO dose on adsorption of FO3R and BPB was investigated in range of 0.05–0.3 g at constant pH = 8.3, 17 °C, fixed amount of dye and contact time = 90 min. The removal percent of both dyes increased by increasing MgO dose which attributed to greater number of active sites of catalyst [4, 28]. The adsorption capacity of FO3R decreased from 32.23 to 7.27 mg g^{-1} which attributed to decrease concentration of dye per mass unit of catalyst. However, the adsorption capacity of BPB increased with increasing amount of MgO nanoparticles as presented in Fig. 7.

Effect of dye concentration

The initial concentration of adsorbate also plays an important role as a given mass of the adsorbent can adsorb only a fixed amount of the solute. Batch adsorption experiments were carried out by shaking the adsorbent with an aqueous solution of the dye of desired concentrations in corning glass bottles. The effect of initial dye concentrations was studied in rang of 17–83 and 1.8–38 mg L^{-1} for FO3R and BPB, respectively. The adsorption capacity of FO3R increased from 8.63 to 33.9 mg g^{-1} and from 4.9 to 28 mg g^{-1} for BPB upon increase in dye concentration as presented in Fig. 8. Several authors reported that dye removal by MgO increased with increase in dye concentration up to optimum value [28]. Others reported that the adsorption efficiency using MgO is independent on initial concentration of dye [29].

Adsorption isotherm model

The equilibrium data of fast orange 3R and bromophenol blue were analyzed by fitting them into Langmuir, Freundlich, Temkin and Dubinin equations to find out the suitable model that may be used for design consideration. Table 2 summarizes the constants and coefficients of different models.

Langmuir isotherm The Langmuir isotherm assumes the absence of any interaction between adsorbate molecules, and the adsorption process is account for monolayer formation on homogeneous adsorbent surface. The linearized form of the Langmuir isotherm is expressed as follows [30]:

$$\frac{C_e}{q_e} = \frac{1}{bq_{max}} + \frac{C_e}{q_{max}}$$

where the q_{max} (mg g^{-1}) is the maximum adsorption capacity of the adsorbent corresponding to monolayer formation and illustrates the maximum value of q_e that can be attained as C_e is increased. The b parameter is a coefficient related to the energy of adsorption and increases with increasing strength of the adsorption bond. Values of q_{max} and b are determined from the linear plot of (C_e/q_e) versus C_e and listed in Table 2. The essential characters of Langmuir isotherm can be expressed in term of dimensionless constant separation factor R_L given by

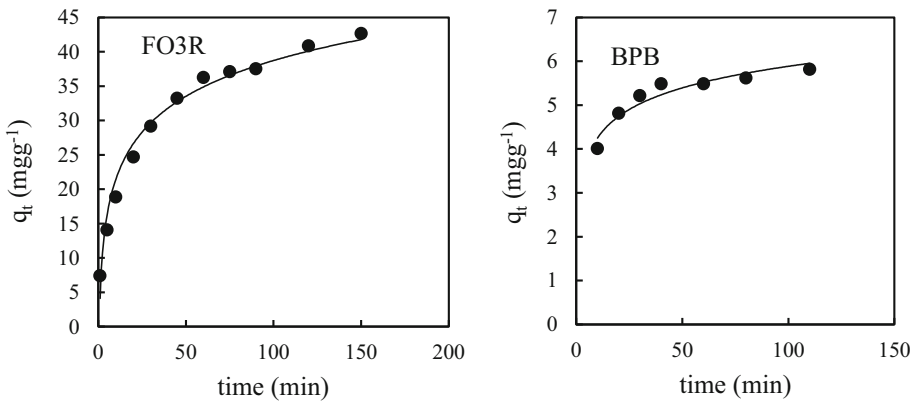

Fig. 6 Effect of contact time on the adsorption of dye. pH = 8.3, Temp. = 12 °C, 0.1 g of MgO

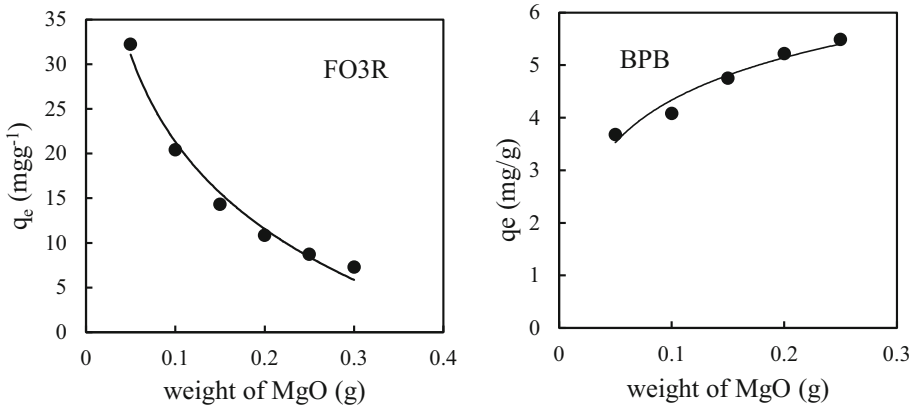

Fig. 7 Effect of MgO dose on adsorption of dye pH = 8.3, Temp. = 17 °C

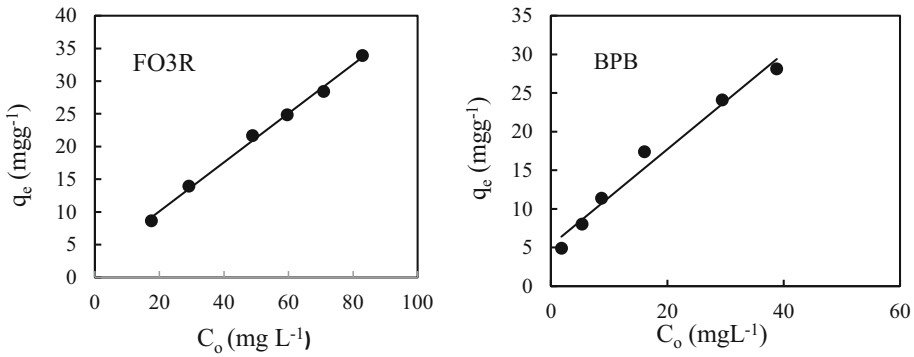

Fig. 8 Effect of dye concentrations on adsorption pH = 8.3, Temp. = 17 °C, 0.1 g MgO

Table 2 Adsorption isotherms parameters of FO3R and BPB on MgO

Adsorption parameters	Fast orange 3R	Bromophenol blue
Langmuir model		
Q_{max} (mg g^{-1})	29.76	40.5
b	0.735	0.05
R^2	0.985	0.945
Freundlich model		
K_f	12.91	3.26
n	3.4	1.70
R^2	0.999	0.994
Temkin model		
α (mg g^{-1}min^{-1})	18.92	1.424
β (g mg^{-1})	4.82	7.74
R^2	0.974	0.929
Dubinin model		
B (J^2 mol^{-2})	7 × 10^{-8}	7 × 10^{-6}
E (J mol^{-1})	2672	267.26
Q_m (mg g^{-1})	22.4	23.38
R^2	0.797	0.867

$$R_L = \frac{1}{1 + bC_o}$$

where, b is Langmuir constant and C_o is initial dye concentration (mg L^{-1}). The value of R_L in the present investigation is found to lie between 0.016–0.074 and 0.340–0.917 for FO3R and BPB, respectively, which indicating that the adsorption is favorable ($0 < R_L < 1$) at the temperature studied.

Freundlich isotherm The Freundlich isotherm considers multilayer adsorption with heterogeneous energetic distribution of active sites accompanied by interaction between adsorbed molecules. The Freundlich equation [31] is expressed as follows in its linearized form:

$$\log q_e = \log K_f + \frac{1}{n} \log C_e$$

where K_f and n are constants. The constant K_f represents the capacity of the adsorbent for the adsorbate, and 1/n shows adsorption intensity of dye on solid which is a function of the strength of adsorption. A linear plot of log q_e versus log C_e gives the K_f and n values and listed in Table 2. Freundlich value $n > 1$ indicates favor adsorption, and the value of R^2 is greater than that obtained from

Langmuir isotherm indicating that Freundlich isotherm model more fit for FO3R and BPB dyes.

Temkin isotherm Temkin isotherm assumes the decline of the heat of sorption as a function of temperature is linear relationship. The linear Temkin [32] equation is

$$q_e = \beta \ln \alpha + \beta \ln C_e$$

α is the equilibrium constant corresponding to the maximum binding energy/L g^{-1}

β is constant related to heat of adsorption, $\beta = RT/b$

b is the Temkin constant related to heat sorption/J mg^{-1}

α and β are calculated from the slope and intercept of plot q_e versus ln C_e and listed in Table 2. The adsorption energy obtained for adsorption of FO3R and BPB onto MgO was 499.38 and 34.9 J mg^{-1} which indicates that the adsorption process is endothermic and a strong interaction between MgO and both dyes.

Dubinin–Radushkevich isotherm The isotherm assumes the surface heterogeneity and the variation of adsorption potential during sorption process [33]. The model has commonly been applied in the following linear equation:

$$\ln q_e = \ln Q_m - B€^2$$

Polanyi potential, €, can be calculated according the following equation

$$€ = RT \ln(1 + 1/C_e)$$

where B is a constant related to the adsorption energy and Q_m the theoretical saturation capacity. The slope of the plot of ln q_e versus $€^2$ gives B (mol^2 kJ^2) and the intercept yields the adsorption capacity, Q_m (mg g^{-1}). The mean free energy of adsorption (E) which is energy required to transfer one mole of the dye from infinity in solution to the surface of the solid can be calculated from the B value using the following relation and is listed in Table 2

$$E = 1/\sqrt{2B}$$

Adsorption kinetics

Adsorption of organic dyes on metal oxide surface is influenced by three mass transfer processes which are external diffusion of dye molecules from liquid phase to the solid surface, intraparticle diffusion of dye molecules in the interior of pores and adsorption to the surface sites (actual adsorption). The actual adsorption process is usually very fast rather than internal and external diffusion. It is well known that the adsorption equilibrium is reached within several minutes. However, the long adsorption equilibrium time suggests that the internal diffusion controls the reaction rate.

Kinetic is key factor for adsorption investigation, it gives clue about the rate of removing the pollutants from aqueous solutions and the mechanism of adsorption process. Several models are available to investigate the adsorption mechanism and description based on experimental data such as pseudo-first order, pseudo-second order, intramolecular diffusion and Elovich models. The pseudo-first-order adsorption rate [34] and pseudo-second-order adsorption rate developed by Ho and McKay [35] have the following linear forms

Pseudo-first-order equation Lagergren proposed a method for adsorption analysis [34] in the form

$$\ln(q_e - q_t) = \ln q_e - k_1 t$$

where q_t is adsorption capacity at time t, q_e is adsorption capacity at equilibrium condition and k_1 is first-order rate constant of adsorption. The adsorption rate constants k_1 and q_e were calculated from the plot of $\log(q_e - q_t)$ versus t and listed in Table 3.

Pseudo-second-order equation The pseudo-second-order adsorption rate equation developed by Ho and McKay [35] has the following linear form

$$\frac{t}{q_t} = \frac{1}{k_2 q_e^2} + \frac{t}{q_e}$$

where k_2 is second-order rate constant of adsorption. Also k_2 and q_e were calculated from the plot of t/q_t versus t and listed in Table 3.

A good linear plot was obtained for pseudo-second-order reaction model rather than pseudo-first order.

Table 3 Adsorption kinetics constants of FO3R and BPB on MgO

Kinetic parameters	Fast orange 3R	Bromophenol blue
Pseudo-first order		
q_e (mg g^{-1}) experimental	38	5.82
q_e calculated	36.37	3.93
k_1 (min^{-1})	0.056	0.081
R^2	0.977	0.985
Pseudo-second order		
q_e calculated	45.04	0.96
k_2 (g mg^{-1} min^{-1})	1.66×10^{-3}	0. 12
R^2	0.994	0.992
Intraparticle		
k_{id} (mg $g^{-1}min^{-0.5}$)	3.96	0.466
C	5.57	2.619
R^2	0.976	0.977
Elovich		
α (mg $g^{-1}min^{-1}$)	8.9	1.45
β (g mg^{-1})	0.116	1.41
R^2	0.9944	0.916

Table 4 Thermodynamic parameters for the adsorption of FO3R and BPB on MgO

T/*K*	K_e/FO3R	K_e/BPB	FO3R	BPB		
			$\Delta G°$/kJ mol^{-1}	$\Delta G°$/kJ mol^{-1}	$\Delta H°$/kJ mol^{-1}	$\Delta S°$/kJmol^{-1}K^{-1}
298	1.56	3.70	−1.092	−3.236	37.82 (FO3R)	0.13
303	1.80	3.92	−1.485	−3.435	7.33 (BPB)	0.035
308	2.11	4.09	−1.906	−3.600		
313	3.32	4.27	−3.119	−3.771		

Intraparticle diffusion The limiting step in dye adsorption may be either the boundary film formation or intraparticle (pore) diffusion of the dye on the solid surface from bulk of solution. Weber and Morris explained the diffusion mechanism through the following equation [36]:

$$q_t = k_{id} t^{1/2} + C$$

C (mg g^{-1}) is the thickness of boundary layer, k_{id} is intraparticle diffusion rate constant (mg g^{-1} min$^{-0.5}$) which are evaluated from the intercept and slope of plot q_t versus $t^{1/2}$ and listed in Table 3. Straight lines are obtained for both dyes adsorption on MgO did not pass through origin. The result indicates that intraparticle diffusion affects the rate of dye removal but it is not only the rate-determining step. The constant 'C' is found to be 5.57 and 2.62 for both adsorptions of FO3R and BPB on MgO, respectively.

Elovich It is rate equation in which the absorbing surface is heterogeneous [37]. It is represented as

$$q_t = \frac{1}{\beta}\ln \alpha\beta + \frac{1}{\beta}\ln t$$

α is the initial adsorption rate(mg g^{-1} min^{-1}), β is the desorption constant (gmg^{-1}) which are calculated from intercept and slope of plot q_t versus ln t and listed in Table 3.

Reichenberg It is another model for investigating the dynamic behavior of the system [38]. It is represented as

$$B_t = -0.4977 - \ln(1 - F)$$

where F is the fractional attainment of equilibrium at different times (t) and B_t is a function of F as follows:

$$F = q_t/q_e$$

where q_t and q_e are the dye uptake (mg g^{-1}) at time t and equilibrium, respectively. The linear plot of B_t versus time is linear and has zero intercept, when the pore diffusion controls the rate of mass transfer. It should be emphasized that nonlinear or linear plots with intercept value different than the zero indicate that film diffusion or chemical reaction may control the adsorption rate. In this study that the relation between B_t and time is linear with very small intercept, 0.629 and 0.378, for adsorption of FO3R and BPB, respectively. This result reveals that intraparticle diffusion of both dyes inside MgO pores may be essential factor in controlling adsorption process.

Adsorption thermodynamics

Adsorption at different temperature usually indicates the favorability of the adsorption process. The effect of temperature on the dye adsorption onto MgO nanoparticles was studied. The obtained data showed that the adsorption capacity increased with increasing the temperature from 298 to 313 K indicating the endothermic nature of dye adsorption. This supports the possibility of chemisorptions of FO3R and BPB with MgO nanoparticles where there is an increase in the number of molecules acquiring sufficient energy to undergo chemical reaction with adsorbent at higher temperature. Thermodynamic parameters such as free energy change ($\Delta G°$), enthalpy ($\Delta H°$) and entropy ($\Delta S°$) are evaluated to confirm the nature of adsorption of FO3R and BPB onto MgO nanoparticles. Thermodynamic parameters are calculated by the Van't Hoff equation

$$\ln K_e = -\frac{\Delta H^\circ}{RT} + \frac{\Delta S^\circ}{R}$$

From the slope and intercept of Van't Hoff plot $\Delta H°$ and $\Delta S°$ were calculated. The Gibbs free energy change $\Delta G°$ was calculated using the following equation and is listed in Table 4.

$$\Delta G^\circ = -RT \ln K_e$$

The positive values of $\Delta H°$ and $\Delta S°$ reveal that the adsorption process is endothermic with increasing the randomness of the system. The negative value of free energy indicates that the adsorption process is spontaneous. Moreover, the value of free energy became more negative with raise in temperature suggesting that the adsorption became more favorable at higher temperatures. This is similar to results reported earlier.

Conclusions

This research work reflects the potentiality of MgO nanorods as an effective and preferential adsorbent for removal of two anionic dyes due to the higher point of zero charge of MgO. The structure, crystalline and morphology

feature of MgO nanoparticles were investigated using XRD, BET, SEM, TEM and HRTEM techniques. TEM results reflect the existence of mesopores of various dimensions which can increase the mass transfer and diffusion of the dye molecules inside these wide pores. The influence of reaction parameters such as initial dye concentration, temperature, catalyst dosage and shaking time on dye adsorption was investigated. The experimental data reflect that the removal FO3R and BPB dye increases with increasing in the contact time, initial dye concentration, catalyst dose and temperature. The strong adsorption ability of the MgO nanoparticles is due to the electrostatic attractions between positive surface of the metal oxide and the anionic dyes. The adsorption capacity increased with increasing the temperature indicating the endothermic nature of dye adsorption. This supports the possibility of chemisorption of FO3R and BPB with MgO nanoparticles. The positive values of ΔH° and ΔS° reveal that the adsorption process is endothermic with increasing the randomness of the system. MgO with rod-like structure can be considered a good candidate for adsorption and removal of various organic pollutants.

References

1. Perullini M, Jobbgy M, Japas ML, Bilmes SA (2014) New method for the simultaneous determination of diffusion and adsorption of dyes in silica hydrogels. J Colloid Interface Sci 425:91–95
2. Pearce CI, Lloyd JR, Guthrie JT (2003) The removal of color from textile wastewater using whole bacterial cells: a review. Dyes Pigments 58:179–196
3. Ferraz ER, Grando MD, Oliveira DP (2011) The azo dye disperse orange 1 induces DNA damage and cytotoxic effects but does not cause ecotoxic effects in Daphnia similis and Vibrio fischeri. J Hazard Mater 192:628–633
4. Moussavi G, Mahmoudi M (2009) Removal of azo and anthraquinone reactive dyes from industrial wastewaters using MgO nanoparticles. J Hazard Mater 168:806–812
5. Han R, Ding D, Xu Y, Zou W, Wang Y, Li Y, Zou L (2008) Use of rice husk for the adsorption of congo red from aqueous solution in column mode. Bioresour Technol 99:2938–2946
6. Abou-Gamra ZM, Medien HA (2013) Kinetic, thermodynamic and equilibrium studies of rhodamine b adsorption by low cost biosorbent sugar cane bagasse. Eur Chem Bull 2(7):417–422
7. Ren B (2014) Electrospinning synthesis of MgO nanofibers and properties of Uranium (VI)-sorption. J Chem Soc Pak 36(2):250–254
8. Abou-Gamra ZM, Ahmed MA (2015) TiO_2 nanoparticles for removal of malachite green dye from Waste Water. Adv Chem Eng Sci 5:373–388
9. Salem M, Ahmed MA, El-Shahat MF (2016) Selective adsorption of amaranth dye on Fe_3O_4/MgO nanoparticles. J Mol Liq 219:780–788
10. Rasulia L, Mahvib AH (2016) Removal of Humic acid from aqueous solution using MgO nanoparticles. J Water Chem Technol 38(1):21–27
11. Sari A, Soylak M (2007) Equilibrium and thermodynamic studies of stearic acid adsorption on Celtek clay. J Serb Chem Soc 72(5):485–494
12. Ghaedi M, Ghobadzadeh P, Nasiri Kokhdan S, Soylak M (2013) Oxidized multiwalled carbon nanotubes as adsorbents for kinetic and equilibrium study of removal of 5-(4-Dimethyl Amino Benzylidene)Rhodanine. Arab J Sci Eng 38:1691–1699
13. Neppolian B, Wang Q, Jung H, Choi H (2008) Ultrasonic-assisted sol-gel method of preparation of TiO_2 nano-particles: characterization, properties and 4-chloro-phenol removal application. Ultrason Sonochem 15:649–658
14. Niu H, Yang Q, Tang K, Xie Y (2006) Self-assembly of porous MgO nanoparticles into coral-like microcrystals. Scr Mater 54:1791–1796
15. Mageshwari K, Mali SS, Sathyamoorthy R, Patil PS (2013) Template-free synthesis of MgO nanoparticles for effective. Powder Technol 249:456–462
16. Nagappa B, Chandrappa GT (2007) Mesoporous nanocrystalline magnesium oxide for environmental remediation. Microporous Mesoporous Mater 106:212–218
17. Rezaei M, Khajenoori M, Nematollahi B (2011) Synthesis of high surface area Nanocrystalline MgO by pluronic P123 triblock copolymer surfactant. Powder Technol 205:112–116
18. Li X, Xiao W, He G, Zheng W, Yu N, Tan M (2012) Pore size and surface area control of MgO nanostructures using a surfactant-templated hydrothermal process: high adsorption capability to azo dyes. Colloids Surf A 408:79–86
19. Venkatesha G, Nayaka YA, Chethana BK (2013) Adsorption of Ponceau S from aqueous solution by MgO nanoparticles. Appl Surf Sci 276:620–627
20. Venkatesha TG, Viswanatha R, Arthoba Y, Chethana BK (2012) Kinetics and thermodynamics of reactive and vat dyes adsorption on MgO nanoparticles. Chem Eng J198–199:1–10
21. Mahmoud HR, El-Molla SA, Saif M (2013) Improvement of physicochemical properties of Fe_2O_3/MgO nanomaterials by hydrothermal treatment for dye removal from industrial wastewater. Powder Technol 249:225–233
22. Wang T, Xu Y, Su Q, Yang R, Wang L, Liu B, Shen S, Jiang G, Chen W, Wang S (2014) Hierarchical porous nanosheet-assembled MgO microrods with high adsorption capacity. Mater Lett 116:332–336
23. Letterman RD, American Water Works Association (1999) Water quality and treatment, 5th edn. McGraw-Hill Inc, New York
24. Bagheri A, Sabbaghan M, Mirgani Z (2015) A comparative study on properties of synthesized MgO with different Templates. Spectrochim Acta Part A Mol Biomol Spectrosc 137:1286–1291
25. Gulkova D, Solcova O, Zdrazil M (2004) Preparation of MgO catalytic support in shaped mesoporous high surface area form. Microporous Mesoporous Mater 76:137–149
26. Gandhi S, Abiramipriya P, Pooja N, Juliat Latha Jeyakumari J, Yelil Arasi A, Dhanalakshmi V, Gopinathan Nair M, Anbarasan R (2011) Synthesis and characterizations of nano sized MgO and its nano composite with poly(vinyl alcohol). J Non Cryst Solids 357:181–185
27. Dhal JP, Sethi M, Mishra BG, Hota G (2015) MgO nanomaterials with different morphologies and their sorption capacity for removal of toxic dyes. Mater Lett 141:267–271
28. Asrari E, Tavallali H, Zare Z (2013) Application of MgO nanocrystals as efficient adsorbent for removal basic dyes. J Appl Sci Environ Sanit 8(4):287–292
29. Richards R, Mulukutla RS, Mishakov I, Chesnokov V, Volodin A, Zaikovski V, Sun N, Klabunde KJ (2001) Nanocrystalline ultra high surface area magnesium oxide as a selective based catalyst. Scr Mater 44:1663–1666
30. Langmuir I (1918) The adsorption of gases on plane surfaces of glass, mica and platinum. J Am Chem Soc 40:1361–1403

31. Freundlich HMF (1906) Over the adsorption in solution. J Phys Chem US 57:385–471
32. Temkin MJ, Pyzhev V (1940) Acta Physiochim URSS 12:217–225
33. Dubinin MM (1965) Modern state of the theory of volume filling of micropore adsorbents during adsorption of gases and steams on carbon adsorbents. Zh Fiz Khim 39:1305–1317
34. Lagergren S (1898) Zur theorie der sogenannten adsorption gelöster stoffe, Kungliga Svenska Vetenskapsakademiens. Handlingar 24:1–39
35. Ho YS, McKay G (1999) Pseudo-second-order model for sorption processes. Process Biochem 34:451–465
36. Weber WJ, Morris JC (1963) Kinetics of adsorption on carbon from solution. J Sanitary Eng Div 89(2):31–60
37. Chien SH, Clayton WR (1980) Application of Elovich equation to the kinetics of phosphate release and sorption on soils. Soil Sci Soc Am J 44:265–268
38. Reichenberg D (1953) J Am Chem Soc 75:589